energies

MDPI

Article

Development of MVMD-EO-LSTM Model for a Short-Term Photovoltaic Power Prediction

Xiaozhi Gao [1], Lichi Gao [1], Hsiung-Cheng Lin [2,*], Yanming Huo [1], Yaheng Ren [3] and Wang Guo [1]

[1] College of Electrical Engineering, Hebei University of Science and Technology, Shijiazhuang 050018, China
[2] Department of Electronic Engineering, National Chin-Yi University of Technology, Taichung 41170, Taiwan
[3] Institute of Applied Mathematics, Hebei Academy of Sciences, Shijiazhuang 050011, China
* Correspondence: hclin@ncut.edu.tw

Abstract: The accuracy and stability of short-term photovoltaic (PV) power prediction is crucial for power planning and dispatching in a grid system. For this reason, the multi-resolution variational modal decomposition (MVMD) method is proposed to achieve multi-scale input features mining for short-term PV power prediction. Here, the MVMD combined with Spearman extracts correlation features of the weather data. An equilibrium optimizer (EO) is integrated with MVMD to achieve optimal values of the long short-term memory (LSTM) parameters. Firstly, the correlation of input features is determined and selected by Spearman. The MVMD model is used to mine the high correlation features of solar radiation and conduct cross-correlation analysis to extract input feature components. Secondly, the similar weather days of the sample set are classified to ensure a good adaptability in different weather situations. Finally, the high correlation features are introduced into the photovoltaic power prediction model of EO optimized LSTM. Performance analysis using actual output power data from a PV plant shows that the proposed MVMD feature extraction method can effectively mine correlation features to achieve an optimized dataset under different seasons. Compared with the gray wolf and particle swarm optimization algorithms, the proposed model has a better optimization performance in a low discrimination of input feature decomposition components and low correlation with output power.

Keywords: solar energy; short-term PV power forecast; multiresolution variational modal decomposition (MVMD); feature extraction; equilibrium optimizer (EO); long short-term memory (LSTM)

Citation: Gao, X.; Gao, L.; Lin, H.-C.; Huo, Y.; Ren, Y.; Guo, W. Development of MVMD-EO-LSTM Model for a Short-Term Photovoltaic Power Prediction. *Energies* **2022**, *15*, 7332. https://doi.org/10.3390/en15197332

Academic Editors: Kun-Mu Lee and Wei-Hao Chiu

Received: 2 August 2022
Accepted: 29 September 2022
Published: 6 October 2022

1. Introduction

With the increasing demand for energy globally, the power generation from photovoltaic (PV) power has been extensively exploited around the world. However, its random, fluctuating and intermittent characteristics can result in a significant impact on the power system's stability and quality when it connects to the large-scale grid [1,2]. For this reason, the prediction of PV power generation has been a hot research topic [3]. In terms of time scale, the prediction can be classified into ultra-short, short-term, medium and long term. Among them, medium and long term forecasts generally require a longer period of time for data collection, used mainly for grid planning, design and dispatch. Ultra-short and short term forecasts can be used particularly for real-time grid dispatch, which is of great importance for ensuring safe and stable grid operation.

Traditional short-term PV power forecasting studies applied time-series forecasting methods for numerical weather data as the input variables and generated power data for the output variables. For instance, references [4,5] used autoregressive moving average model (ARMA) and autoregressive integrated moving average model (ARIMA) for power prediction. Unfortunately, directly taking environmental factors and historical data as the input variables may make the model have a lower applicability and robustness. In reference [6], a support vector machine (SVM) regression model was established

using temperature, dew point, humidity, wind speed, time and historical photovoltaic power data as the inputs. The one-hour ahead prediction was realized under unknown irradiance in two weather conditions, fair and cloudy. On the other hand, reference [7] analyzed the influencing PV output power factors using the Pearson correlation coefficient method. The results indicated that solar irradiance, ambient temperature, wind speed and humidity were significantly correlated to PV predictions. In reference [8], the PV power and its influencing factors were decomposed by wavelet, and the decomposition results were used as the input variables to establish an artificial neural network (ANN) PV power prediction model. Apart from wavelet transform, variational modal decomposition (VMD)was widely applied in PV power signal decomposition to overcome the modal aliasing phenomenon [9]. Reference [10] used VMD to decompose photovoltaic power data, thus improving the grasshopper algorithm (GOA)-nuclear limit learning machine (KELM) (GOA-KELM). However, the single-layer VMD has insufficient features for mining long-time data, and KELM has some limitations in the correlation of time series. Refs. [11,12] proposed a wavelet packet decomposition (WPD) model to overcome the shortcomings of single-layer decomposition, but the adaptability was still insufficient due to the inherent limitations of wavelet transform.

In recent years, deep learning algorithms, represented by LSTM, have been widely applied in the PV power prediction [13]. Refs. [14,15] combined particle swarm optimization (PSO) and gray wolf optimizer (GWO) algorithms to optimize LSTM parameters in short-term PV power prediction. However, PSO is prone to produce premature convergence and fall into a local optimum solution. Moreover, GWO may present low accuracy and slow convergence speed when there are many optimization-seeking parameters involved. On the other hand, EO proposed by Afshin Faramarzi et al. in 2019 has superiority over traditional intelligent algorithms on several test functions [16]. In reference [17], the EO algorithm was employed to solve the optimal tide calculation problem of hybrid AC–DC grids, and the calculation results on four objectives such as generation cost, pollutant emission, network loss and voltage offset showed that the EO algorithm has a better optimization performance than the differential evolution algorithm and PSO algorithm.

2. Data Preprocessing Based on MVMD for Feature Extraction

Traditional decomposition algorithms such as fast Fourier decomposition (FFT), empirical mode decomposition (EMD), composite empirical mode decomposition (EEMD), wavelet packet decomposition (WPD), variational mode decomposition (VMD), etc., may suffer from dividing the spectrum interval according to only local extreme spectrum points [8–12]. Apart from overcoming the shortcomings as above, the proposed MVMD decomposition model can reduce the interference of large amplitude clutter components caused by strong background noise in the spectrum, and suppress the problem of mode aliasing. Combined with the multi-resolution analysis architecture, it can also avoid excessive dispersion of effective information, and achieve a more flexible and detailed division of the entire spectrum interval of the signal.

Firstly, Spearman correlation analysis method is used to calculate the correlation coefficient between each influencing factor and photovoltaic output power, screen the influencing factors with high correlation coefficient and then decompose the influencing factors through MVMD to obtain the characteristic components, so as to increase the number of input characteristics. Finally, K-means is used to establish corresponding training sets for different types of weather.

2.1. Spearman Correlation Analysis Method

The Spearman correlation analysis method is applied to determine the correlation between the characteristics of non-linear, non-normal distribution PV dataset. It can be calculated as follows:

$$\rho = \frac{\sum_{i=1}^{n} (x_i - \overline{x})(y_i - \overline{y})}{\sqrt{\sum_{i=1}^{n} (x_i - \overline{x})^2 \sum_{i=1}^{n} (y_i - \overline{y})^2}} \tag{1}$$

where n is the sample size; ρ is the correlation coefficient; x, y are the corresponding elements in the two variables. In practical applications, the link between the variables is irrelevant, which can be calculated in a simple step:

$$r_s = 1 - \frac{6 \sum_{i=1}^{n} d_i^2}{n^3 - n} \tag{2}$$

$$d_i = R(x_i) - R(y_i) \tag{3}$$

where r_s is the rank correlation coefficient; $R(x_i)$ and $R(y_i)$ are the ranks of x_i and y_i, respectively; d_i is the position after the ranking. The strength of correlation is determined by the value of r_s: the closer it is to 0, the weaker the correlation is.

2.2. Fundamentals of MVMD Algorithm

The MVMD algorithm takes VMD as the core decomposition algorithm and combines with multi-resolution decomposition architecture. The number K of VMD decomposition at each layer is a fixed value (K = 2) to prevent effective information from being too scattered. To balance computation amount and computation speed, the number of decomposition layers is set as 3 (L = 3). As shown in Figure 1, H_1 and L_1 are decomposition components using VMD decomposition in the first layer of the original signal, and then H_1 and L_1 are decomposed to obtain HH_1, HL_1, L_{H1} and L_{L1} by VMD again. Components obtained by VMD decomposition of each layer is used as input signals of the next layer decomposition, where K value of each decomposition is set as 2. Therefore the original signal S can be expressed as:

$$S = IF_1 + IF_2 + IF_3 + IF_4 + IF_5 + IF_6 + IF_7 + IF_8 \tag{4}$$

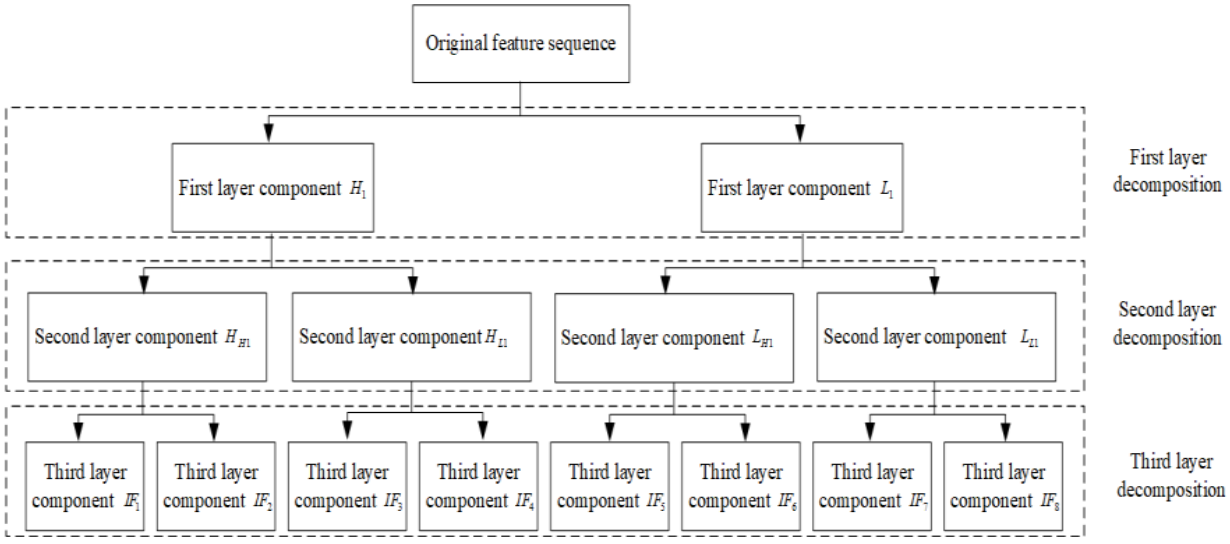

Figure 1. Architecture of MVMD decomposition.

In this paper, the solar radiation, which has the highest correlation with the output power, is taken as the decomposition object and its wave characteristics are further excavated. Meanwhile, in order to avoid feature redundancy, the Spearman correlation analysis method is adopted to evaluate the correlation and cross-correlation of the decomposition components obtained by MVMD (Equations (1) and (2)) and screen them. Finally, in order to further improve the prediction accuracy, K-means is used to carry out similar day clustering and establish datasets corresponding to different types of weather.

3. LSTM Power Prediction Model Based on EO Algorithm

The EO belongs to the meta heuristic optimization algorithm, and it is simple, independent of the problem, flexible and gradient free with better universality [16]. Comparing EO with existing optimization methods such as PSO and GWO algorithms based on single mode, multi-mode, combined functions and engineering application problems, the EO algorithm is highly effective in obtaining optimal or near optimal solutions [16–18]. Therefore, this study adopted the EO algorithm to optimize LSTM parameters.

3.1. EO Algorithm

The algorithm optimization model using the EO algorithm is described as follows:

(1) Population particle initialization

The initial population is used to start the optimization process. The initial concentrations are constructed based on the number of particles and dimensions with uniform random initialization in the search space, as follows:

$$\vec{C}_i^0 = \vec{C}_{\min} + \vec{r}_i\left(\vec{C}_{\max} - \vec{C}_{\min}\right), i = 1, 2 \ldots, N \tag{5}$$

where $\hat{r}_i$ is random vector between [0,1], $i \in [i, N]$; N is population particle quantity; $\vec{C}_{\max}$ is upper bound of the search space; $\vec{C}_{\min}$ is lower bound of search space;

(2) Construct the equilibrium pool and select the candidate solution

When the equilibrium state is not reached in the early iteration, the candidate solution is used to determine the particle search mode. In the whole optimization process, the fitness value of each particle is calculated, and four particles with optimal fitness and the average value of these four particles are identified as candidate solutions to form an equilibrium pool:

$$\vec{C}_{eq,pool} = \left\{\vec{C}_{eq(1)}, \vec{C}_{eq(2)}, \vec{C}_{eq(3)}, \vec{C}_{eq(4)}, \vec{C}_{eq(ave)}\right\} \tag{6}$$

where $\vec{C}_{eq(ave)} = \frac{\vec{C}_{eq(1)}+\vec{C}_{eq(2)}+\vec{C}_{eq(3)}+\vec{C}_{eq(4)}}{4}$. In the equilibrium pool, the probability of each particle used as a solution to guide the optimization process is 0.2;

(3) Exponential term (F)

In order to balance the global search and local search of the algorithm and ensure the convergence of the algorithm, the index is set as follows:

$$\vec{F} = a_1 sign\left(\vec{r} - 0.5\right)\left[e^{-\vec{\lambda}t} - 1\right] \tag{7}$$

where $t = 1 - \left(\frac{Iter}{Max\_iter}\right)^{a_2 \frac{Iter}{Max\_iter}}$; a_1 and a_2 are constant; $Iter$ and Max_iter are the number of current iterations and the maximum number of iterations, respectively; $\vec{\lambda}$ is a random vector between [0,1] whose dimension is the same as the dimension of the optimized space;

$\text{sign}\left(\vec{r} - 0.5\right)$ represents the function used to control the direction of exploration and development;

(4) Generation rate (G)

To enhance the local optimization capability of the algorithm, the MVMD generation rate is designed as follows:

$$\vec{G} = \vec{G}_0 e^{-\vec{\lambda}(t-t_0)} = \vec{G}_0 \vec{F} \tag{8}$$

$$\vec{G}_0 = \vec{GCP}\left(\vec{C}_{eq} - \vec{\lambda}\vec{C}\right) \tag{9}$$

$$\vec{GCP} = \begin{cases} 0.5r_1 r_2 \geq GP \\ 0r_2 < GP \end{cases} \tag{10}$$

where $\vec{C}_{eq}$ is a randomly selected solution from the equilibrium pool; $\vec{GCP}$ is the control parameter of generation rate G, when GP = 0.5, the algorithm achieves balance between global optimization and local optimization.

To sum up, the final update formula of EO is as follows:

$$\vec{C} = \vec{C}_{eq} + \left(\vec{C} - \vec{C}_{eq}\right)\vec{F} + \frac{\vec{G}}{\vec{\lambda} V}\left(1 - \vec{F}\right) \tag{11}$$

$\vec{C}_{eq}$ represents the concentration of guide particles selected from the equilibrium pool. $\left(\vec{C} - \vec{C}_{eq}\right)\vec{F}$ is added to find the optimal solution in the global search space by using the concentration difference between sample particle $\vec{C}$ and equilibrium particle $\vec{C}_{eq}$. Through $\vec{F}$, the EO can achieve a reasonable balance between exploration and development. Here, $\frac{\vec{G}}{\vec{\lambda} V}\left(1 - \vec{F}\right)$ produces a small change in concentration through the formation rate $\vec{G}$, which makes the result more accurate.

3.2. The Procedure of EO Optimizing LSTM Parameter

The settings of learning rate, number of iterations and number of neurons in the hidden layer of the LSTM model have a direct impact on the results of PV power prediction accuracy. The learning rate and the number of iterations have a large impact on the training effect of the model, the number of neurons in the hidden layer plays a decisive role in the degree of fit of the model and these parameters have a large randomness [19–21]. Parameter selection by hand cannot guarantee the prediction effect of the model, so the LSTM parameters are selected by using the EO algorithm with a strong merit-seeking ability and fast convergence speed. The EO-LSTM process is described as follows:

(1) Divide the dataset into a training set and a test set;
(2) The number of iterations and learning rate of hidden layer neurons in LSTM are used as the object of EO optimization, i.e., the information of each particle concentration is a three-dimensional vector representing the number of hidden layer neurons, the number of iterations and the learning rate;
(3) To guarantee global optimization results, the generation rate of EO algorithm GP is set as 0.5, and constant a_1 = 2 and a_2 = 1 [16]. Considering the convergence speed and time cost of the algorithm, the number of iterations T is set as 100 and the number of particles K is set as 30. $C_{\max} = [300, 0.01, 300]$ and $C_{\min} = [100, 0.002, 100]$ are the upper and lower limits of the particle search space, and the fitness function *F(x)* is the mean absolute error (*MAE*) of predicted value and output value in the photovoltaic power;
(4) Random initialization is carried out in the search space through Equation (5);

(5) The concentration information of each particle was imported into LSTM network, and the corresponding fitness value was calculated by training and prediction through the training set;

(6) Compare the fitness values of each particle, filter out the four particles with the smallest fitness values as $\vec{C}_{eq(1)}$, $\vec{C}_{eq(2)}$, $\vec{C}_{eq(3)}$, $\vec{C}_{eq(4)}$. At the same time, calculate the mean concentration $\vec{C}_{eq(ave)}$ of these four particles to construct the equilibrium pool $\vec{C}_{eq,pool}$;

(7) Update the coefficient of exponential term $\vec{F}$ by Equation (7);

(8) Randomly select guide particles $\vec{C}_{eq}$ from the equilibrium pool, and update the generation rate $\vec{G}$ according to Equation (8);

(9) Combine the guiding particle $\vec{C}_{eq}$, the updated pointing coefficient $\vec{F}$ and the generation rate $\vec{G}$. The concentration of each particle is updated one by one through Equation (11);

(10) Judge whether the maximum number of iterations is reached. If the maximum number of iterations is reached, T, output the particle with the lowest fitness in the balance pool, and assign its corresponding parameters to LSTM for model training and prediction in combination with training set and test set; otherwise, return to Step (5).

4. The MVMD-EO-LSTM Model

The flowchart of the proposed MVMD-EO-LSTM model performance for short-term photovoltaic power prediction is shown in Figure 2. The detailed process is demonstrated as follows.

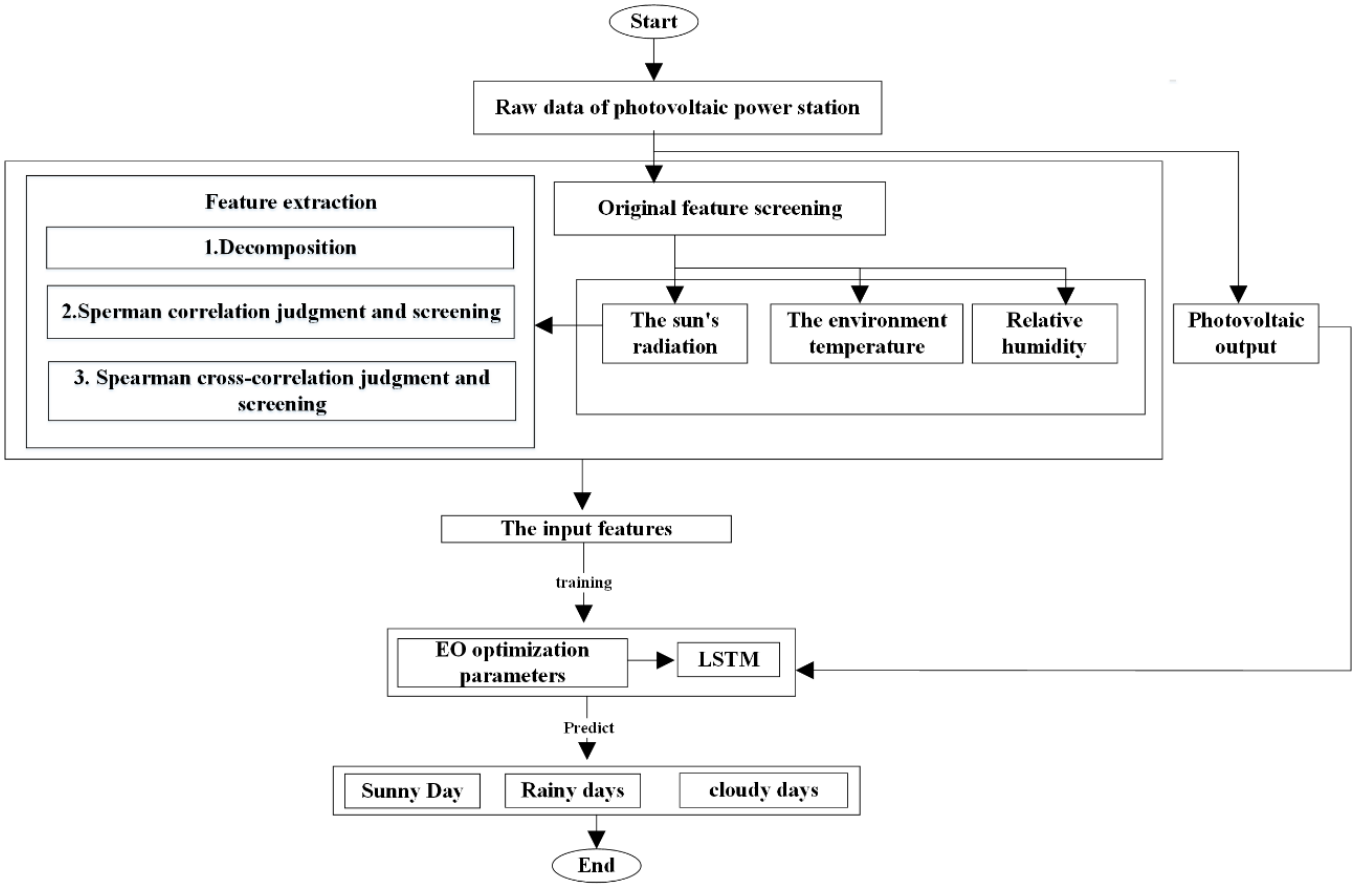

Figure 2. Flowchart of the proposed model performance.

The overall model performance process is illustrated as follows:

(1) Spearman is used to screen the correlation of input features of historical photovoltaic power station data to eliminate the low-correlation features;
(2) MVMD is used to decompose the solar radiation sequence;
(3) Spearman is used to calculate the correlation coefficient between each decomposition component and the output power, screening out the strong correlation component;
(4) The strong correlation components are analyzed by cross-correlation number, grouped and screened as feature extraction results;
(5) The feature extraction results are combined with the original feature screening results as the input feature of the prediction model, and the photovoltaic power is used as the output feature. The dataset is selected based on the K-means similar day clustering result, and the EO-LSTM is used for training and parameter optimization to achieve the photovoltaic power prediction under different weather conditions.

5. Performance Analysis

In this paper, the historical data provided by Ningxia Taiyangshan PV Power Station, China were used as the test object, which were collected for a total of 92 days in June, July and August in a single year. It contained one output power data and six meteorological data (solar radiation, temperature, humidity, pressure, wind speed and wind direction). Considering the intermittent characteristics of PV output power, the daily 5:30–19:00 time period was intercepted, with 54 points per day and the sampling interval was15min, i.e., a total of 4968 sampled points. The computer to implement the proposed model was configured as a Windows 10 Intel (R) Core (TM) i5-8265U CPU (Acer, Taipei, Taiwan). The running time using the Matlab (2020a, MathWorks, USA) took 51,535 s. Note that the overall model operation time can be reduced further if it is performed on a dedicated server.

5.1. Results of Spearman Analysis

The correlation between meteorological factors and PV output power was analyzed by Spearman method. According to Table 1, the correlation between solar radiation and photovoltaic power generation is 0765, confirming this as the greatest influential factor. On the other hand, the correlation coefficients on ambient temperature and relative humidity are 0.41 and −0.339, respectively, showing a moderate correlation with photovoltaic power. However, relative humidity is negatively correlated with photovoltaic power. It implies that photovoltaic power will decrease with the increase in humidity. Moreover, the correlation of air pressure and wind speed over photovoltaic power is almost zero so that it can be discarded in practice.

Table 1. Spearman correlation coefficient between meteorological factors and photovoltaic power generation.

Input Features	Solar Radiation	Environmental Temperature	Relative Humidity	Air Pressure	Wind Speed	Wind Direction
Spearman	0.765	0.410	−0.339	0.086	−0.068	−0.007

5.2. Feature Extraction Results

In order to fully mine the fluctuation characteristics between solar radiation and output power, this study applied an MVMD algorithm to decompose the solar radiation sequence data and obtain 14 components for the multi-resolution refinement and time-frequency localization analysis. Considering the balance of calculation amount and operation speed, the number of decomposition layers was selected as L = 3, the number of components as K = 2 and the convergence criterion r = 1×10^{-7}. The above three parameters values were widely used in the MVMD model to achieve satisfactory outcomes. On the other hand, increasing the penalty factor (α) can reduce the bandwidth of the mode, but there is a high risk of incorrect mode central frequency being captured. If α is too low, the decomposed

modes may contain more noise. In this study, alpha is selected as α = 2500 to reach the compromise. For comparison, the solar radiation was also decomposed using WPD and VMD. Simultaneously, Spearman method was used to analyze the correlation between the decomposition components of each model and the output power.

It can be seen from Figure 3 that there are six decomposition components for MVMD with a correlation coefficient higher than the threshold value, i.e.,0.5 as the threshold, but only three for both VMD and WPD. It reveals that the correlation between the overall decomposition components and the power sequence can be improved by MVMD. As shown in Figure 3, L_1 and H_1 are the decomposition results of the first layer, L_{H1}–H_{L2} are the decomposition results of the second layer and IF_1–IF_8 are the decomposition results of the third layer.

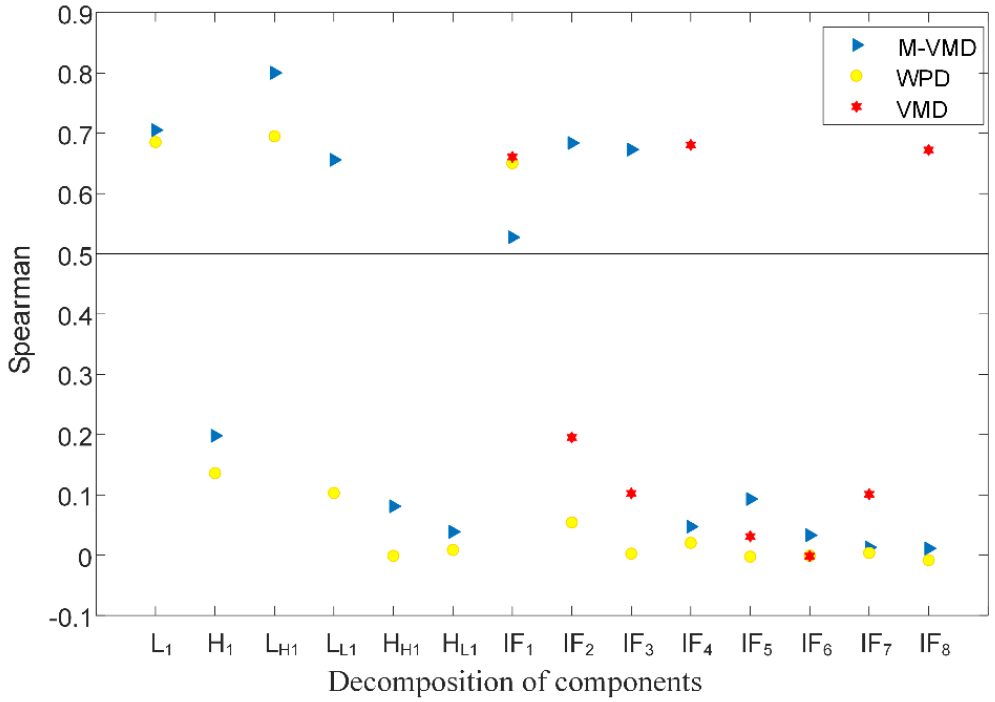

Figure 3. Scatter plot of Spearman decomposition components and output power correlation coefficient of different models.

Figure 4 demonstrates the heat map of the cross-correlation analysis using Spearman for six decomposition components of the MVMD. It can be seen that L_1–L_{H1}, L_{H1}–IF_1, L_{L1}–IF_2, L_{L1}–IF_3 and IF_2–IF_3 have very high cross-correlation coefficients. Cross -correlation coefficients greater than 0.9 can be grouped together, and above six decomposition components can be divided into two groups (group 1: L_1, L_{H1} and IF_1; group 2: L_{L1}, IF_2 and IF_3). The component in each group with highest correlation coefficient with output power is selected as the feature extraction result. From Figure 3, we see that the selected component in group 1 is L_{H1} with correlation coefficient as 0.8, and IF_2 in group 2 with correlation coefficient as 0.68. It indicates that the MVMD feature extraction results are L_{H1} and IF_2, where the cross-correlation coefficient between L_{H1} and IF_2 is 0.54.

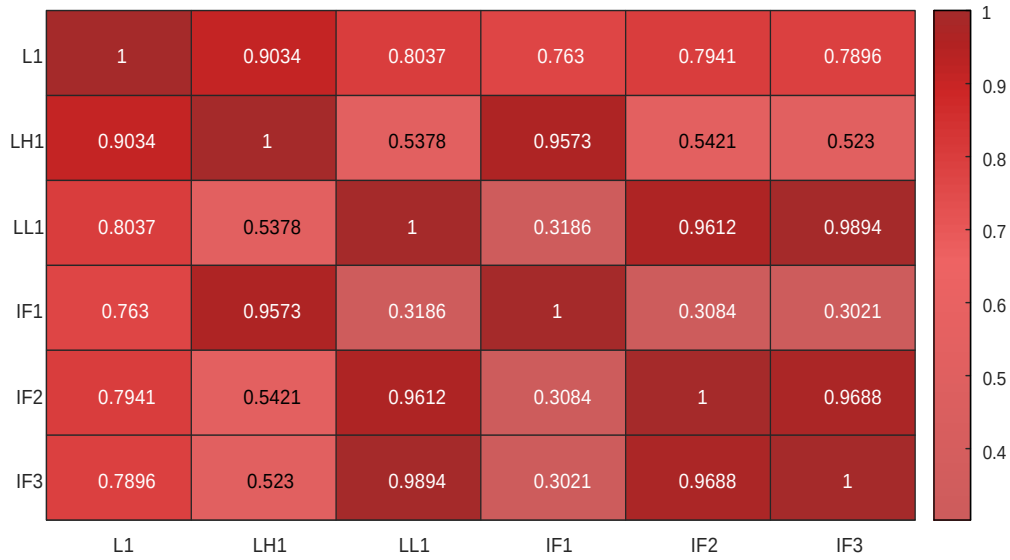

Figure 4. Heat map of solar radiation cross-correlation analysis.

Combined with Table 2, the autocorrelation and cross-correlation are used to screen the decomposition results of VMD and WPD successively. The feature extraction results of VMD are IF_1 and IF_4, and their correlation coefficient is 0.55. The cross-correlation between the three components of WPD is above 0.9, indicating that the three components are a group, and the correlation coefficient between L_1 and the output power is the largest. Therefore, the result of WPD feature extraction is L_1, indicating that the WPD method has the mode aliasing problem. In summary, MVMD can reduce the clutter interference of the spectrum effectively, ensuring the discrimination and recognition among the decomposed components.

Table 2. Cross-correlation analysis of highly correlated features based on WPD and VMD.

Decomposition Method	Characteristic Components	Cross-Correlation
WPD	L_1–L_{H1}	0.994
	L_1–IF_1	0.988
	L_{H1}–IF_1	0.992
VMD	IF_1–IF_4	0.582
	IF_1–IF_8	0.558
	IF_4–IF_8	0.979

Considering photovoltaic (PV) power data are greatly influenced by the weather conditions, this article selects solar radiation, ambient temperature correlation and PV power as the K-means clustering index for similar day. The optimal cluster number K value depends on the elbow coefficient method and the contour. Elbow method takes the sum of squares of errors (SSE) as the core indicator:

$$SSE = \sum_{i=1}^{K} \sum_{p \in C_i} |p - m_i|^2 \tag{12}$$

where C_i represents class I (total class K) of the PV power sample; p is all sample points in C_i; m_i is the mean vector of the class i sample.

The formula of contour coefficient S is as follows:

$$S = \frac{1}{N}\sum_{N}^{i} S(i) = \frac{1}{N}\sum_{N}^{i=1} \frac{b(i) - a(i)}{\max(a(i), b(i))} \tag{13}$$

where a is the average distance of other samples in the same category; b is the average distance of samples in the adjacent category; N is the total number of samples; $S \in [-1, 1]$. The higher the contour coefficient S score is, the better the achievements of the clustering effect.

Based on the k-value from 1 to 10, the corresponding SSE and contour coefficient for each k-value cluster, the results are shown as Figure 5. Figure 5a indicates that the degree of aggregation of various categories increases significantly when k is less than 3, with the increase in the K value, that is, SSE decreases greatly. When k is greater than 3, the result is the opposite. We can see that the inflection point of the elbow diagram is K = 3. Combined with Figure 5b, it can be seen that when K = 3, the contour coefficient is the highest. Therefore, K = 3 is selected for K-means similar day clustering. The clustering results are shown in Table 3.

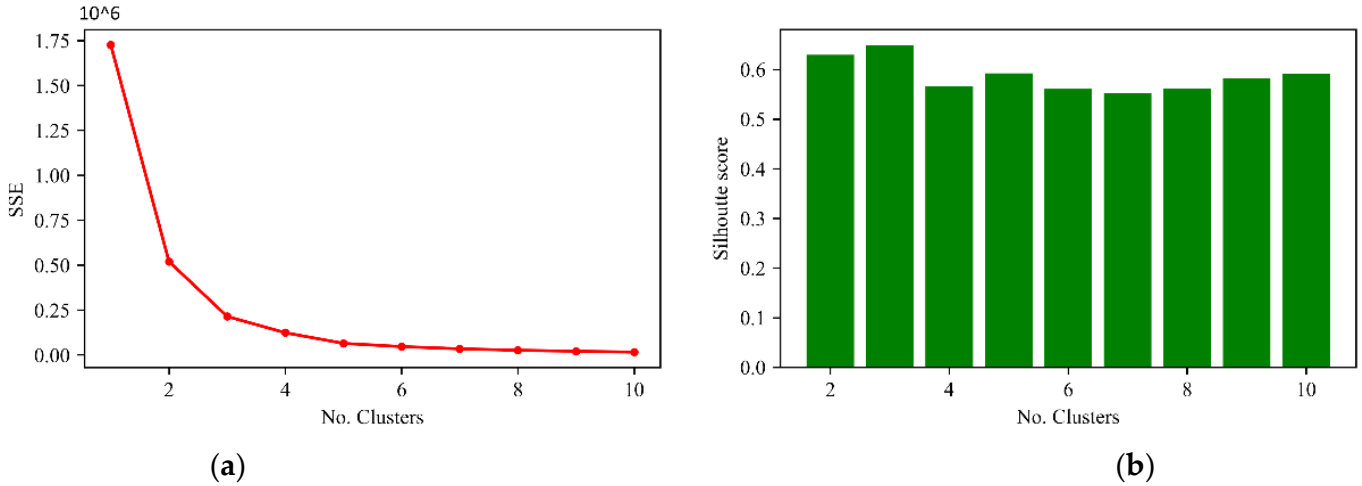

Figure 5. SSE and contour coefficient corresponding to different K value; (**a**) SSE values corresponding to different K values; (**b**) Contour coefficient corresponding to different K value.

Table 3. The number of days in the weather category at K = 3.

Weather Types	Sunny	Cloudy	Rainy
Number of days	51	31	10

5.3. Verification of MVMD Feature Extraction

The original feature and the extraction results by MVMD, VMD and WPD worked as the input of EO-LSTM prediction model, as shown in Table 4. The parameters of models with different inputs are all optimized by EO. *RMSE* and *MAE* are used to evaluate the model accuracy for short-term PV power prediction [22–25].

Table 4. The input features in each model.

Models	Input Features
MVMD	MVMD decomposition feature extraction results (L_{H1} and IF_2), solar irradiation intensity, ambient temperature, relative humidity
VMD	VMD decomposition feature extraction results (IF_1 and IF_4), solar irradiation intensity, ambient temperature, relative humidity
WPD	WPD feature extraction results (L_1), solar irradiation intensity, ambient temperature, relative humidity
Original	Solar irradiation intensity, ambient temperature, relative humidity

Mean Absolute Error (*MAE*) is expressed as:

$$MAE = \frac{1}{n}\sum_{i=1}^{n}|y_i - \hat{y}_i| \tag{14}$$

Root Mean Square Error (*RMSE*) is expressed as:

$$RMSE = \sqrt{\frac{1}{n}\sum_{i=1}^{n}(y_i - \hat{y}_i)^2} \tag{15}$$

where y_i and $\hat{y}_i$ are the actual power value and the predicted power value of the ith sample point, respectively.

The performance evaluation of model prediction using *RMSE* and *MAE* is shown in Tables 5 and 6, respectively. Output comparison under different weather conditions is shown in Figure 6.

Table 5. *RMSE* of each model under different weather conditions.

Models	***RMSE***		
	Sunny	**Cloudy**	**Rainy**
MVMD	0.82709	0.93497	0.74021
VMD	0.95949	1.1857	0.93611
WPD	0.99308	1.5635	1.0313
Original	1.3219	1.7705	1.3491

Table 6. *MAE* of each model under different weather conditions.

Models	***MAE***		
	Sunny	**Cloudy**	**Rainy**
MVMD	0.69789	0.69694	0.56436
VMD	0.75892	0.99214	0.723
WPD	0.80592	1.2282	0.88054
Original	0.83864	1.2836	0.91566

Some points are concluded as follows:

(1) Compared with only original features input, all feature extraction methods (VMD, WPD and MVMD) can improve the prediction accuracy. Among them, the MVMD model presents the best performance, where the mean *RMSE* decreases by 0.64 and the mean *MAE* decreases by 0.35;

(2) Compared with VMD and WPD models, the mean *RMSE* and mean *MAE* for the three weather conditions of the MVMD model were reduced by at least 18%. It exhibited that MVMD can better refine and decompose the input characteristics of photovoltaic power data, indicating that it is more conducive to mining the fluctuation characteristics of the data in the PV power prediction.

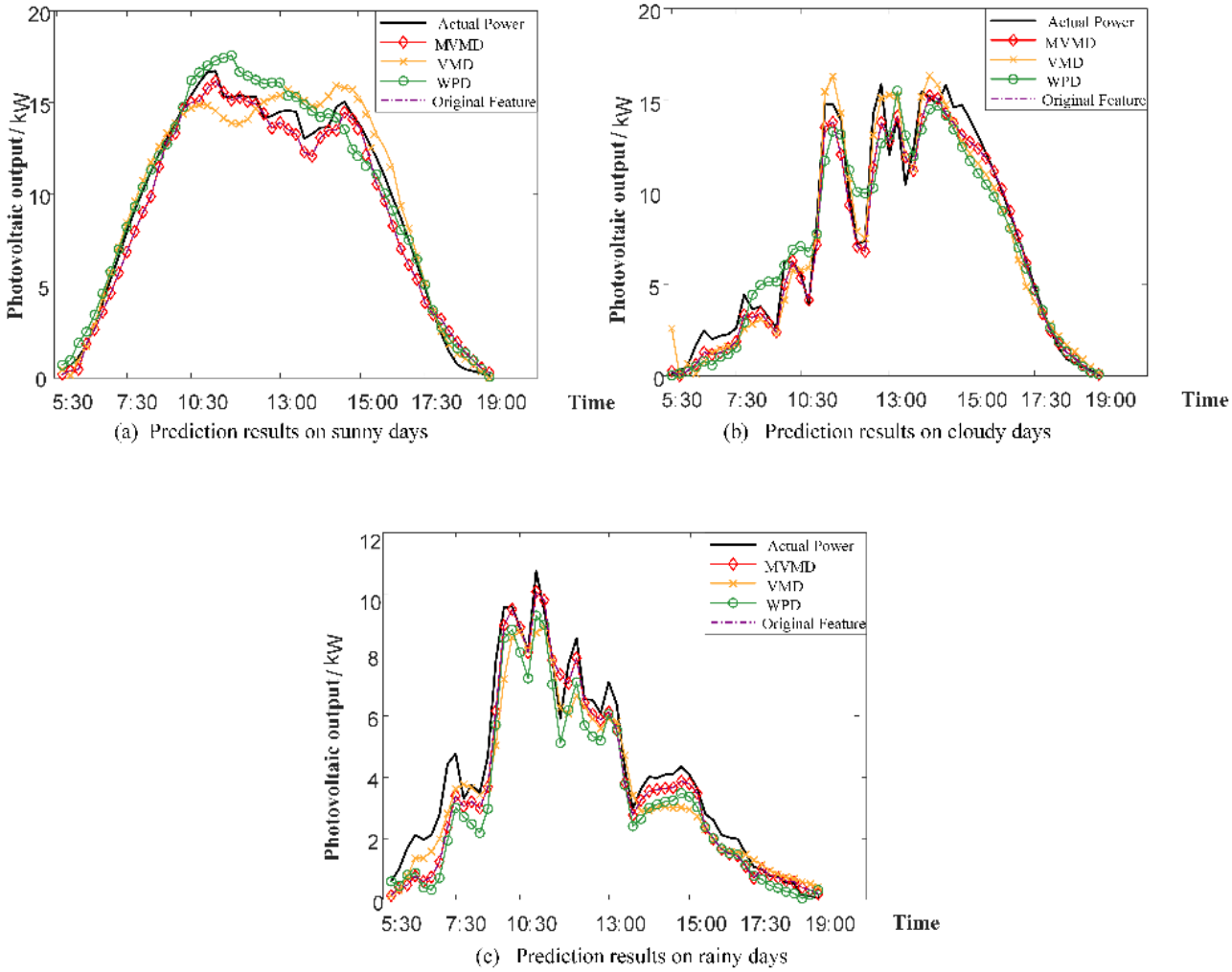

Figure 6. Comparison of each model prediction under different weather conditions.

5.4. Comparison of Optimization Algorithms

In this paper, MVMD feature extraction results and screened original features are used as input datasets, and LSTM parameters are optimized by PSO, GWO and EO algorithms, respectively. The upper and lower limits of each model are: $\vec{C}_{\max} = [300, 0.002, 300]$ and $\vec{C}_{\min} = [100, 0.01, 100]$, and the dimension is set as 3. The prediction results using different optimization algorithms are shown in Tables 7 and 8 and Figure 7.

Table 7. *RMSE* of each optimization model under different weather conditions.

Input	*RMSE*		
	Sunny	**Cloudy**	**Rainy**
EO-LSTM	0.82709	0.93497	0.74021
PSO-LSTM	0.88802	1.0711	0.82262
GWO-LSTM	0.90334	1.0947	0.8284

Table 8. *MAE* of each optimization model under different weather conditions.

Models	*MAE*		
	Sunny	**Cloudy**	**Rainy**
EO-LSTM	0.65789	0.69694	0.56436
PSO-LSTM	0.66806	0.89498	0.65755
GWO-LSTM	0.7632	0.83247	0.55425

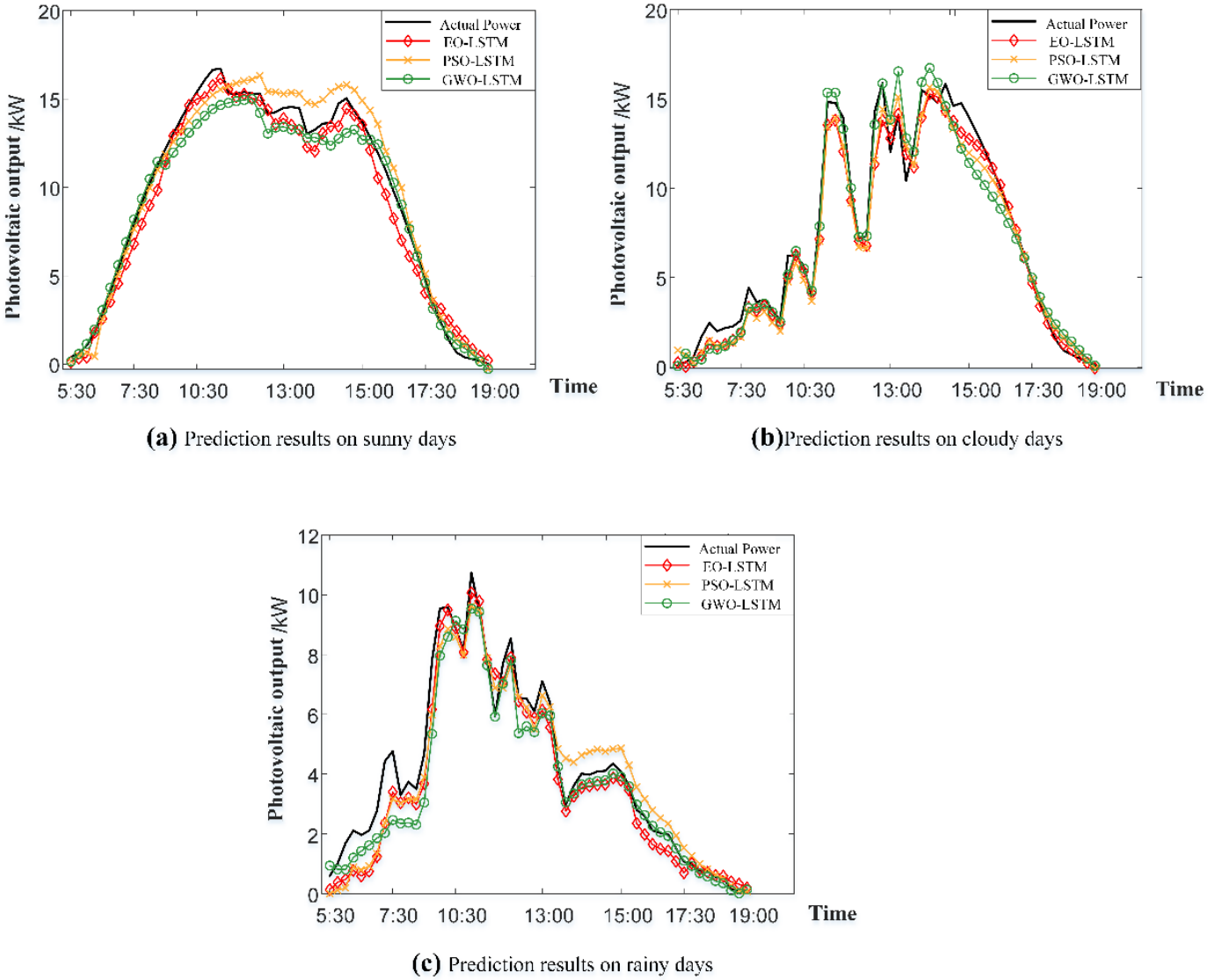

Figure 7. Power prediction of each optimization model in different weather conditions.

It can be seen from Tables 7 and 8 that all three models can achieve satisfactory results under different weather conditions. Compared with PSO-LSTM and GWO-LSTM, the EO-LSTM model has the lowest PV power prediction error, and the mean *RMSE* and *MAE* are reduced by at least 10%. Moreover, the *MAE* value is only 0.56 on rainy days. In Figure 7, it can be seen that EO-LSTM shows good stability and robustness and has good optimization ability for LSTM parameters under different weather conditions, which can effectively improve the prediction accuracy of photovoltaic power.

6. Conclusions

In this study, a short-term PV power prediction model using MVMD-EO-LSTM algorithm based on the feature process from the influence of solar radiation on photovoltaic power output has been performed successfully under three weather conditions: sunny, cloudy and rainy. Some major contributions are concluded as follows:

(1) For non-stationary photovoltaic historical data, the MVMD feature extraction method based on the fusion of VMD and WPD decomposition can effectively build up the relationship between input features and photovoltaic output power. This realizes the fine division of features so that the accuracy and stability in the short-term photovoltaic power prediction can be promised;

(2) By way of EO algorithm with a strong global search ability and high process convergence, LSTM parameters can be determined to optimize the MVMD model. Compared with existing algorithms, the proposed method has better optimization performance, stronger stability and robustness under different weather conditions.

Author Contributions: All authors contributed to this work; Conceptualization and methodology, X.G. and L.G.; software and validation, Y.H. and Y.R.; writing, W.G. and H.-C.L.; visualization, L.G. All authors have read and agreed to the published version of the manuscript.

Funding: Authors would like to acknowledge the funding of the Key Projects of Hebei Province Science and Technology Support Program, grant number 19214501D, the funding of the Science and Technology Research Project of Colleges and Universities in Hebei Province, grant number QN2022028 and the funding of the Scientific Research Project of Hebei Academy of Sciences, grant number 22A01.

Conflicts of Interest: The authors declare no conflict of interest.

References

1. Colak, M.; Yesilbudak, M.; Bayindir, R. Daily Photovoltaic Power Prediction Enhanced by Hybrid GWO-MLP, ALO-MLP and WOA-MLP Models Using Meteorological Information. *Energies* **2020**, *13*, 901. [CrossRef]
2. Serrano Ardila, V.M.; Maciel, J.N.; Ledesma, J.J.; Ando Junior, O.H. Fuzzy Time Series Methods Applied to (In)Direct Short-Term Photovoltaic Power Forecasting. *Energies* **2022**, *15*, 845. [CrossRef]
3. Scolari, E.; Reyes-chamorro, L.; Sossan, F.; Paolone, M. A comprehensive assessment of the short-term uncertainty of grid-connected PV systems. *IEEE Trans. Sustain. Energy* **2018**, *9*, 1458–1467. [CrossRef]
4. Liu, H.K.; Feng, J.X.; Yang, S.Q.; Jia, T. Wind power prediction model based on ARMA and improved BP-ANN. *Adv. Mater. Res.* **2014**, *1008–1009*, 183–187. [CrossRef]
5. Biswas, A.K.; Ahmed, S.I.; Bankefa, T.; Prakash, R.; Salehfar, H. Performance Analysis of Short and Mid-Term Wind Power Prediction using ARIMA and Hybrid Models. In Proceedings of the 2021 IEEE Power and Energy Conference at Illinois (PECI), Urbana, IL, USA, 1–2 April 2021.
6. Nguyen, R.; Yang, Y.; Tohmeh, A.; Yeh, H.-G. Predicting PV Power Generation using SVM Regression. In Proceedings of the IEEE Green Energy and Smart Systems Conference, Long Beach, CA, USA, 1–2 November 2021; pp. 1–5.
7. Kim, G.G.; Choi, J.H.; Park, S.Y.; Bhang, B.G.; Nam, W.J.; Cha, H.L.; Park, N.S.; Ahn, H.K. Prediction Model for PV Performance With Correlation Analysis of Environmental Variables. *IEEE J. Photovolt.* **2019**, *9*, 832–841. [CrossRef]
8. Wang, S.; Zhang, Y.; Wang, Z.; Cui, F.; Wang, S. A Power Prediction Method for PV system Based on Wavelet Decomposition and Neural Networks. In Proceedings of the 2020 IEEE/IAS Industrial and Commercial Power System Asia (I&CPS Asia), Weihai, China, 13–16 July 2020.
9. Zhao, Y.; Li, C.; Fu, W.; Liu, J.; Chen, H. A modified variational mode decomposition method based on envelope nesting and multi-criteria evaluation. *J. Sound Vib.* **2020**, *468*, 115099. [CrossRef]
10. Sun, W.; Wang, A.; Zhang, T. Short-Term Photovoltaic Power Interval Prediction Based on VMD and GOA-KELM Algorithms. In Proceedings of the 2021 IEEE 4th International Conference on Electronics Technology (ICET), Chengdu, China, 7–10 May 2021.
11. Ye, R.; Guo, Z.; Liu, R.; Liu, J. Short-term wind speed forecasting method based on wavelet packet decomposition and improved Elman neural network. In Proceedings of the 2016 International Conference on Probabilistic Methods Applied to Power Systems (PMAPS), Beijing, China, 16–20 October 2016.
12. Yin, J.; Perakis, A.N.; Wang, N. An Ensemble Real-Time Tidal Level Prediction Mechanism Using Multiresolution Wavelet Decomposition Method. *IEEE Trans. Geosci. Remote Sens.* **2018**, *56*, 4856–4865. [CrossRef]
13. Li, Y.; Ye, F.; Liu, Z.; Wang, Z.; Mao, Y. A Short-Term Photovoltaic Power Generation Forecast Method Based on LSTM. *Math. Probl. Eng.* **2021**, *2021*, 6613123. [CrossRef]

14. Ren, X.Q.; Liu, S.L.; Yu, X.D.; Dong, X. A method for state-of-charge estimation of lithium-ion batteries based on PSO-LSTM. *Energy* **2021**, *234*, 121236. [CrossRef]
15. Zhao, H.; Zhao, Z.; Wang, H.; Yue, Y. Short-term Photovoltaic Power Prediction based on DE-GWO-LSTM. In Proceedings of the 2020 IEEE International Conference on Mechatronics and Automation (ICMA), Beijing, China, 13–16 October 2020.
16. Faramarzi, A.; Heidarinejad, M.; Stephens, B.; Mirjalili, S. Equilibrium optimizer: A novel optimization algorithm. *Knowl.-Based Syst.* **2020**, *191*, 105190. [CrossRef]
17. Dalia, T.A.; Abdullah, M.S.; Waleed, A.S.; Walaa, I.G.; Ragab, A.E. Equilibrium optimizer based multi dimensions operation of hybrid AC/DC grids. *Alex. Eng. J.* **2020**, *59*, 4787–4803.
18. Hossain, M.S.; Mahmood, H. Short-Term Photovoltaic Power Forecasting Using an LSTM Neural Network and Synthetic Weather Forecast. *IEEE Access* **2020**, *8*, 172524–172533. [CrossRef]
19. Shi, M.; Xu, K.; Wang, J.; Yin, R.; Wang, T.; Yong, T. Short-Term Photovoltaic Power Forecast Based on Long Short-Term Memory Network. In Proceedings of the 2019 IEEE 3rd International Electrical and Energy Conference (CIEEC), Beijing, China, 7–9 September 2019.
20. Bates, J.M.; Granger, C.W. The Combination of Forecasts. *Oper. Res. Soc.* **1969**, *20*, 451–468. [CrossRef]
21. Eseye, A.T.; Zhang, J.; Zheng, D. Short-term Photovoltaic Solar Power Forecasting Using a Hybrid Wavelet-PSO-SVM Model Based on SCADA and Meteorological Information. *Renew. Energy* **2018**, *18*, 357–367. [CrossRef]
22. Myers, J.I.; Well, A.D. *Research Design and Statistical Analysis*; Routledge: London, UK, 2003; pp. 305–309.
23. Willmott, C.J.; Matsuura, K. Advantages of the Mean Absolute Error (MAE) Over the Root Mean Square Error (RMSE) in Assessing Average Model Performance. *Clim. Res.* **2005**, *30*, 79–82. [CrossRef]
24. Krishna, V.B.; Wadman, W.S.; Kim, Y. Now Casting: Accurate and Precise Short-Term Wind Power Prediction Using Hyper-local Wind Forecasts. In Proceedings of the Ninth International Conference on Future Energy Systems, Karlsruhe, Germany, 12–15 June 2018.
25. Lorenz, E.; Hurka, J.; Heiemann, D. Irradiance Forecasting for the Power Prediction of Grid-connected Photovoltaic Systems. *IEEE J. Sel. Top. Appl. Earth Obs. Remote Sens.* **2009**, *2*, 2–10. [CrossRef]